

## Supplementary Material

# The effect of Ni-modified LSF<sub>CO</sub> promoting layer on the gas produced through co-electrolysis of CO<sub>2</sub> and H<sub>2</sub>O at intermediate temperatures

Massimiliano Lo Faro \*, Sabrina Campagna Zignani, Vincenzo Antonucci and Antonino Salvatore Aricò

Institute of Advanced Energy Technologies “Nicola Giordano” (ITAE) of the Italian National Research Council (CNR), Via Salita S. Lucia sopra Contesse 5, 98126 Messina, Italy; zignani@itae.cnr.it; vincenzo.antonucci@itae.cnr.it; arico@itae.cnr.it

\* Correspondence: lofaro@itae.cnr.it; Tel.: +39-090-624-243

The polarization curves conducted in the temperature range 525–800 °C revealed an increase in ohmic constrain compared to the bare cell investigated under similar conditions [1]. This increase is due to the additional layer coated to the cathode.

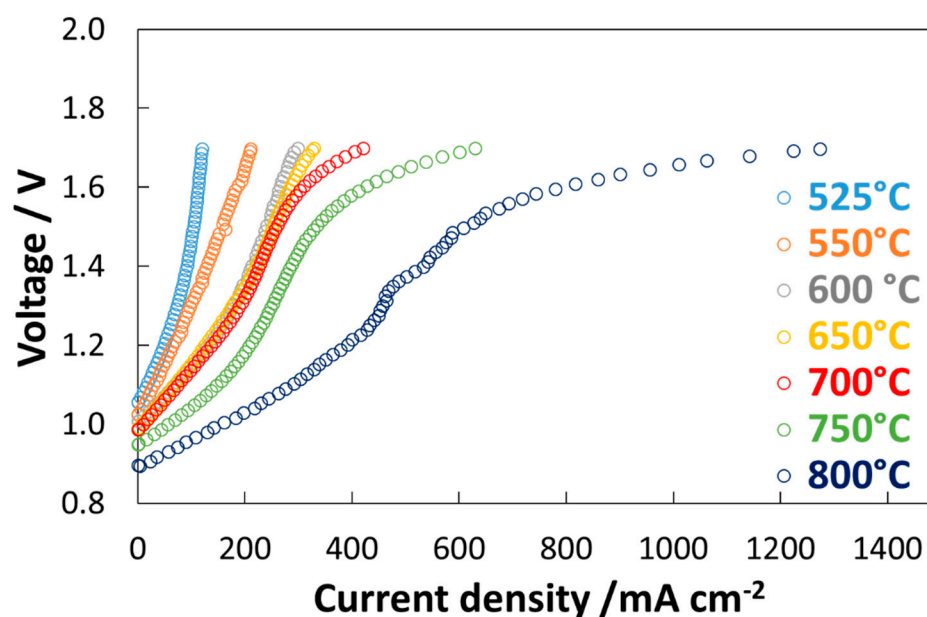


**Figure S1.** Polarization curves of the coated cell investigated in the temperature range 525–800 °C for the co-electrolysis of H<sub>2</sub>O and CO<sub>2</sub>.

The Figure 2S shows the impedance spectra of cell at open circuit voltage (OCV). In OCV conditions, a limited current density was circulated in the cell as that derived from the variation of 10 mV around the OCV value. The increased temperature affected positively both the series resistance ( $R_s$ , intercept with X-axis at high frequencies) and the total resistance ( $R_t$ , intercept with the x-axis at low frequencies). In particular, it is observed a strong effect of the temperature on the semicircle appearing at low frequencies. Low frequency semicircle is related to the reaction characterised by slow kinetics. Although further tests are necessary to uniquely assign each semicircle to each reaction, our previous papers have ascribed to the anodic reaction (oxygen evolution) the low frequency semicircle [2,3].

Citation: Lo Faro, M.; Zignani, S.C.; Antonucci, V.; Aricò, A.S. The effect of Ni-modified LSF<sub>CO</sub> promoting layer on the gas produced through co-electrolysis of CO<sub>2</sub> and H<sub>2</sub>O at intermediate temperatures. *Catalysts* 2021

Received: 20 November 2020

Accepted: 29 December 2020

Published: date

**Publisher's Note:** MDPI stays neutral with regard to jurisdictional claims in published maps and institutional affiliations.



**Copyright:** © 2020 by the authors. Licensee MDPI, Basel, Switzerland. This article is an open access article distributed under the terms and conditions of the Creative Commons Attribution (CC BY) license (<http://creativecommons.org/licenses/by/4.0/>).

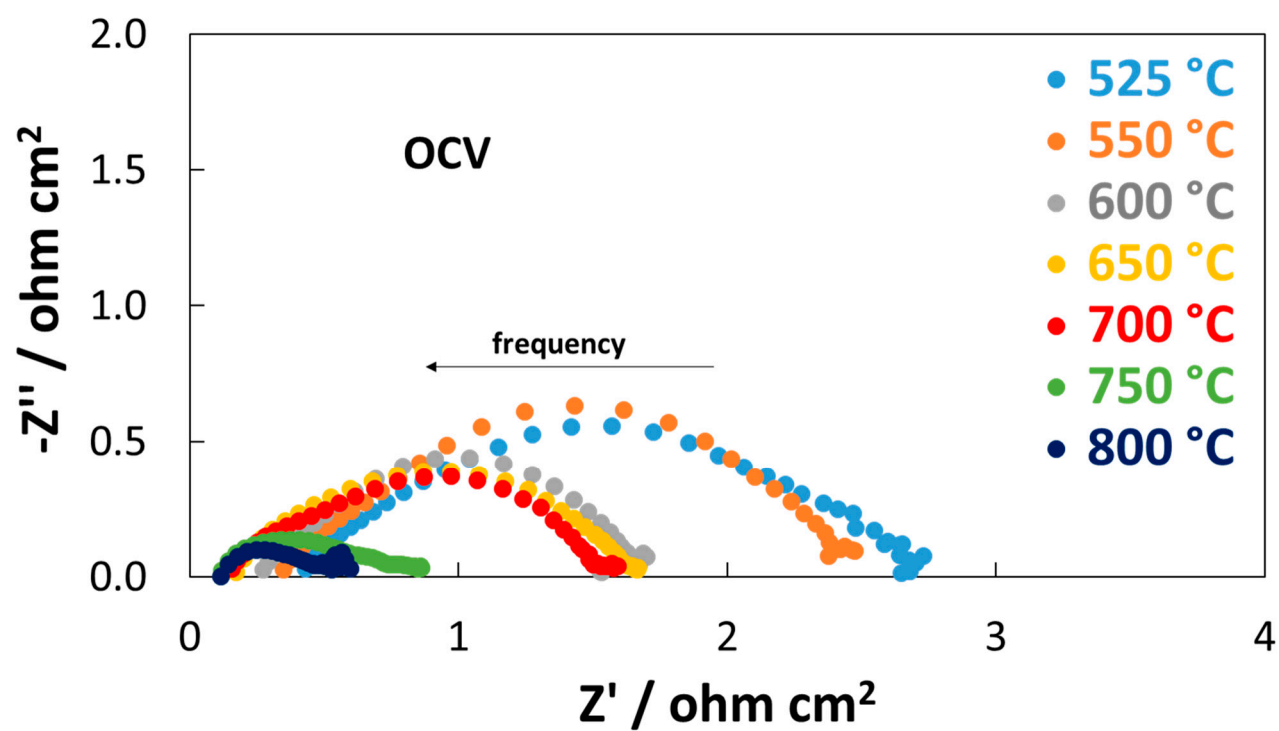


**Figure S2.** Impedance spectra of the coated cell investigated at OCV in the temperature range 525–800 °C for the co-electrolysis of H<sub>2</sub>O and CO<sub>2</sub>.

A similar trend with the temperature was observed for the EIS analysis conducted at 1.3 V. Nevertheless, at below temperatures, just a barely third semicircle was observed at high frequencies as a consequence of the different kinetics for reducing H<sub>2</sub>O and CO<sub>2</sub>.

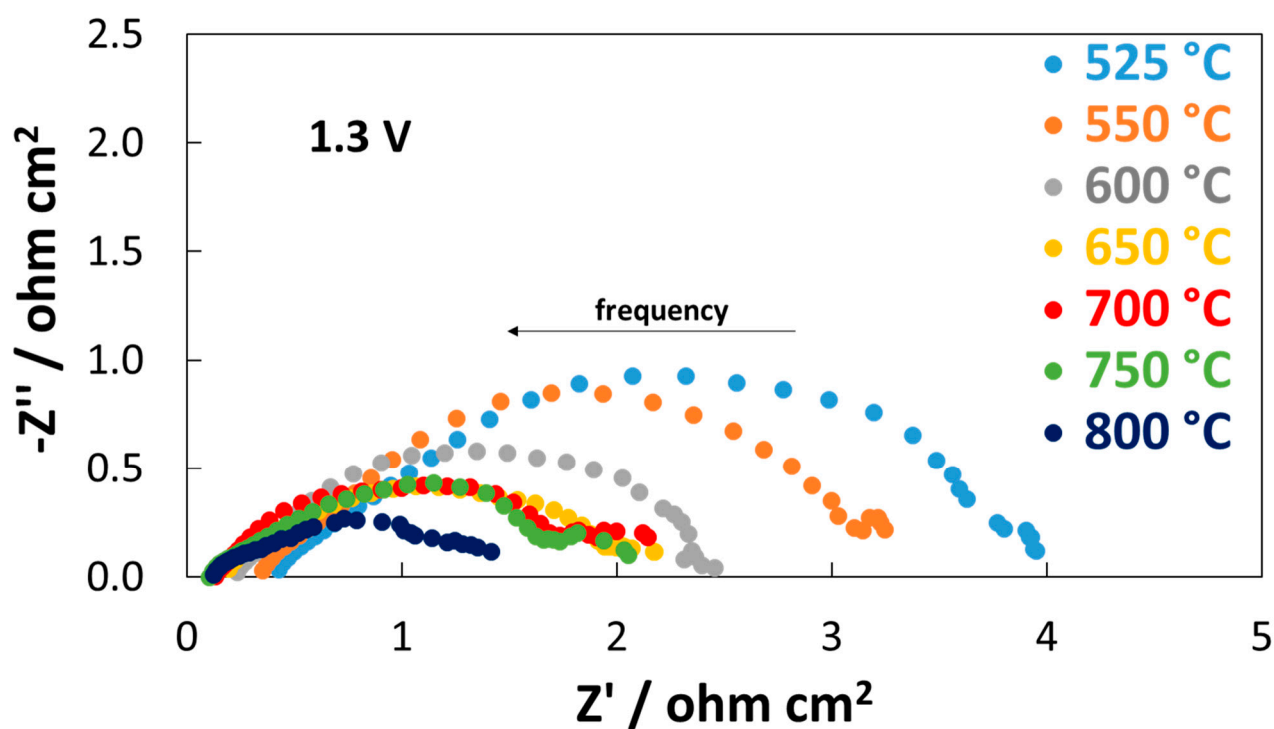


**Figure S3.** Impedance spectra of the coated cell investigated at 1.3 V in the temperature range 525–800 °C for the co-electrolysis of H<sub>2</sub>O and CO<sub>2</sub>.

In Figure S4 and S5 are reported the gas-chromatograms of cell operating at 150 mA cm<sup>-2</sup> and under OCV. These chromatograms were achieved using a Molsieve column (S4) and a Pore-Plot Q (S5) which are suitable for the separation of permanent gases and low weighted hydrocarbons, respectively.

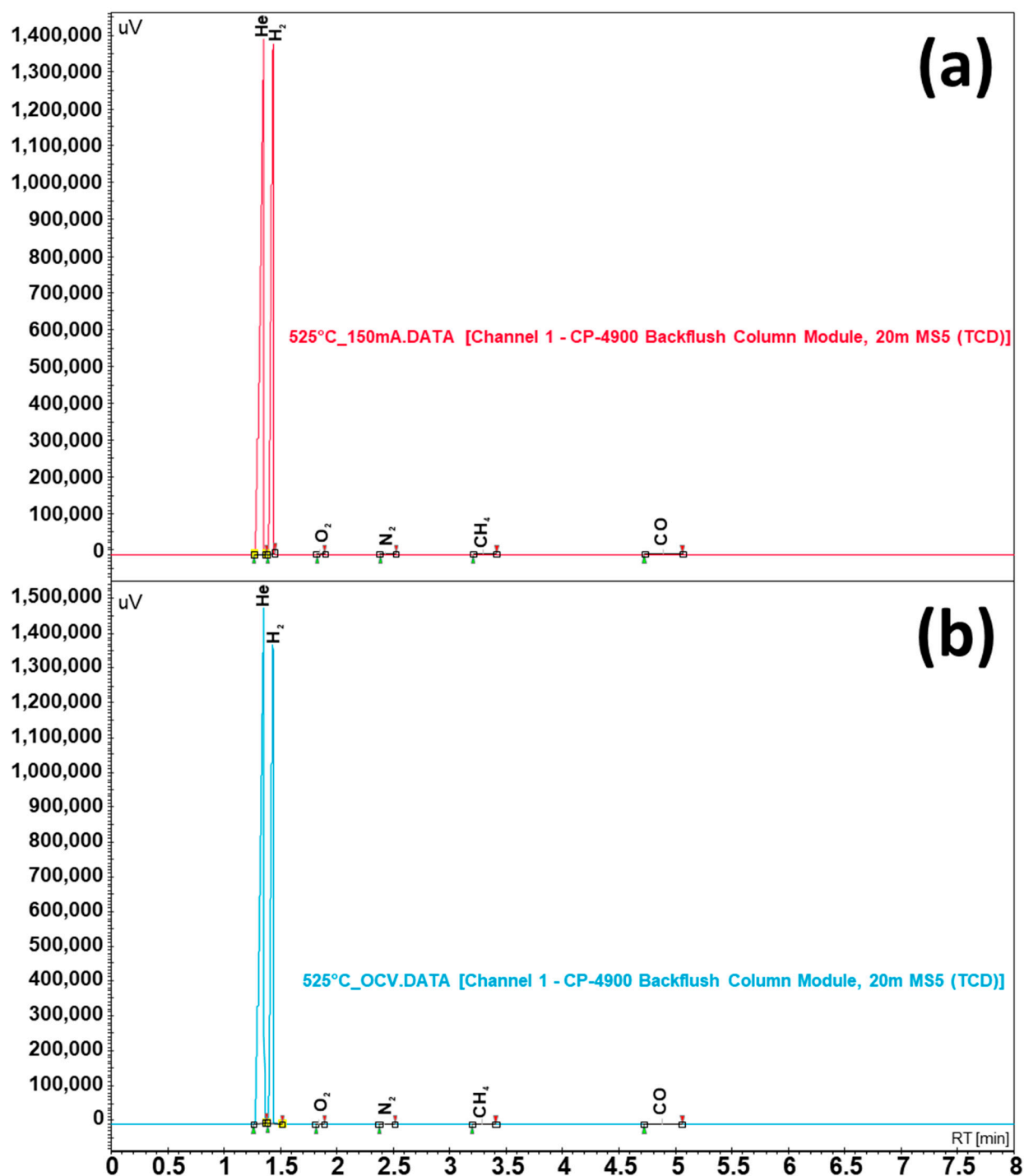


**Figure S4.** Analytes separated with a Molsieve Column and revealed with TCD. Gas-Chromatograms of outlet from cathode chamber of cell operating at 525 °C operating at 150 mA  $\text{cm}^{-2}$  (a) and under OCV (b).

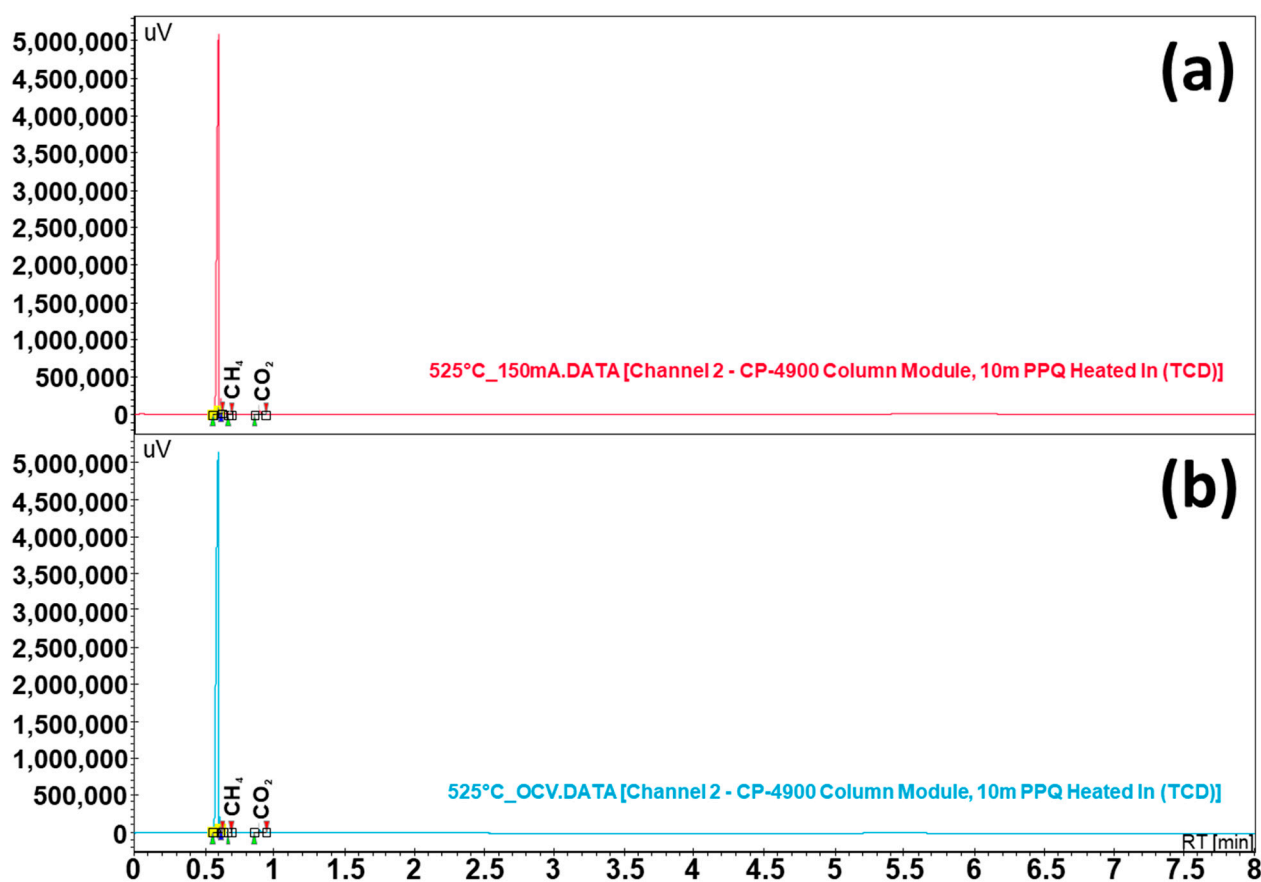


**Figure S5.** Analytes separated with a Pore-Plot Q Column and revealed with TCD. Gas-Chromatograms of outlet from cathode chamber of cell operating at 525 °C operating at 150 mA cm<sup>-2</sup> (a) and under OCV (b).

The gas-chromatographic data concerning C-based molecules were treated according to the following equation:

$$\text{Carbon balance} = \frac{CO_{out} + CO_{2out} + CH_{4out}}{CO_{2in}} \cdot 100 \quad (1)$$

As observed in the Figure S6, the carbon balance represented by the bar chart was close to 100%. This result was an indication of goodness for the gas sealing of cell.

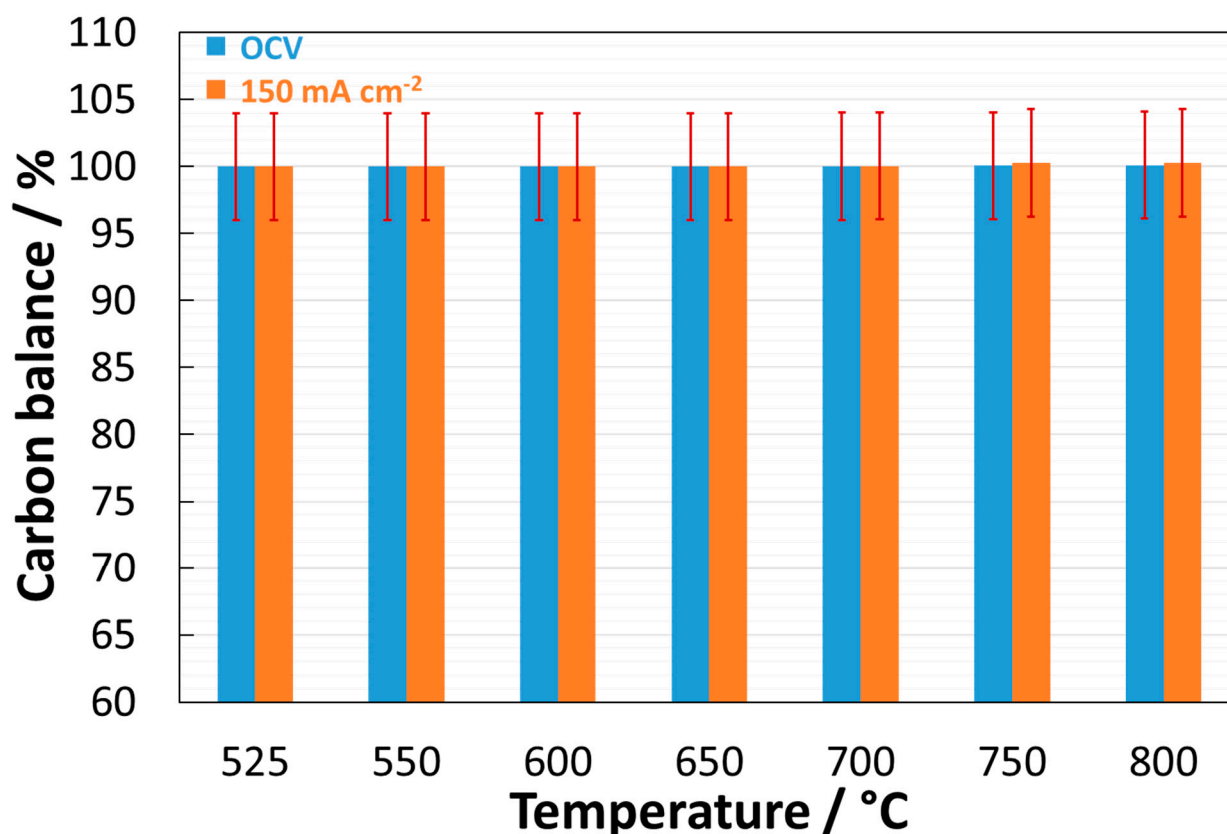


**Figure S6.** Carbon balance of gas achieved under practical conditions. The gas-chromatographic data were treated accordingly to Equation (1).

The Figure S7 shows the SEM image of spent cell. The two magnifications demonstrated that the microstructure was not damaged from the temperature treatment and SOEC operation. It is worthy to note that no delamination occurred, especially at the anode-electrolyte interface, as it is one of the most known drawbacks of these cells (Figure S4a). Another significant information was the absence of carbon deposits on the microporosity of cathode layer.

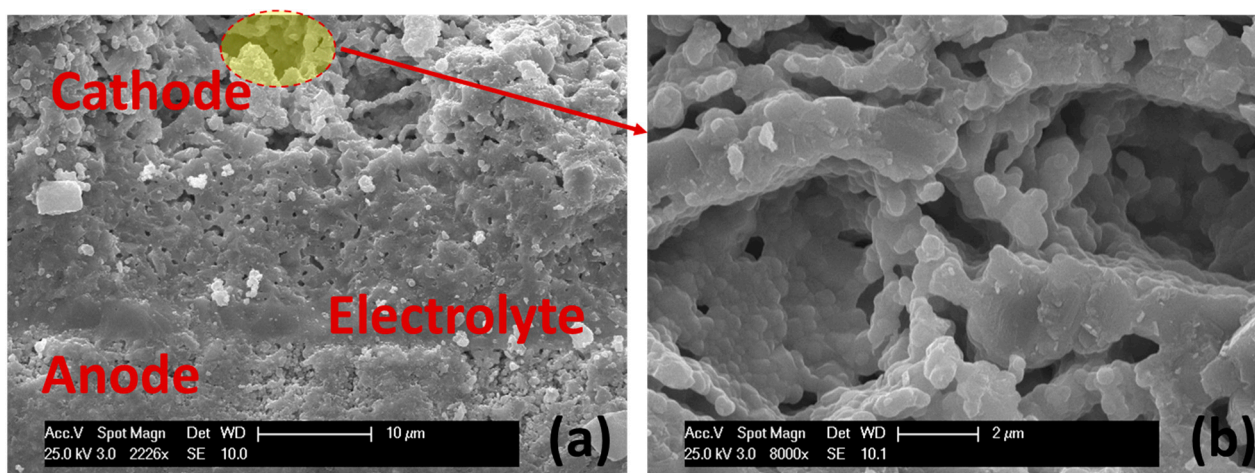


**Figure S7.** SEM analysis of spent cell highlighting the interface regions (a) and the magnification of cathode microstructure (b).

The Figure S8 shows the XRD spectrum of functional layer of spent cell. This material is showing narrow peaks ascribed to CGO and the three further phases generated from the exsolution of perovskite and corresponding to the depleted perovskite with Ruddlesden-Popper structure[4–6], a tri-metallic alloy (e.g., Ni–Fe–Co) and a mixed oxide (e.g.,  $\alpha$ - $\text{Fe}_{100-y-z}\text{Co}_y\text{Ni}_z\text{O}_x$ ) [7,8].

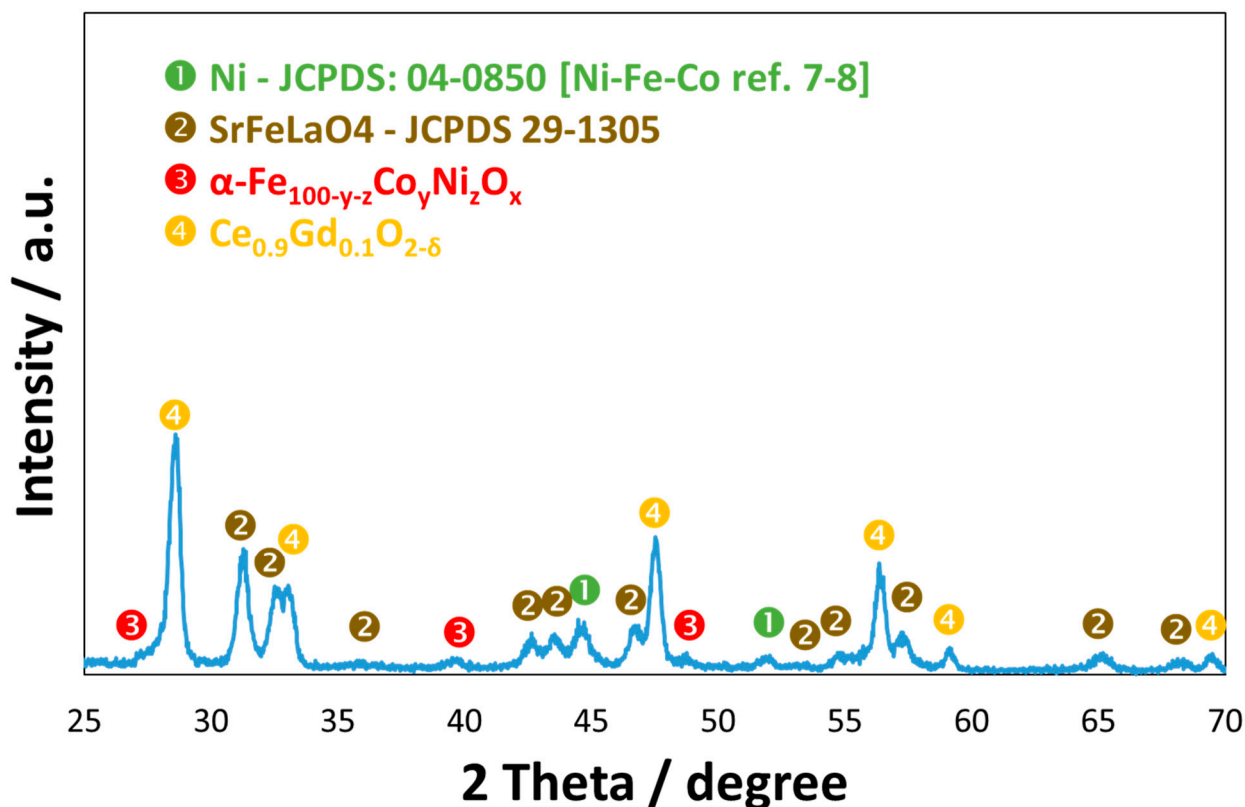


Figure S8. XRD spectrum of functional layer on the spent cell.

A further investigation of spent functional layer consisted of the HR-TEM analysis shown in Figure S9. The morphology of the specimen appeared complex since many phases were recognised. Nevertheless, EDX analysis is showing as the Ni-based encapsulated phase was well distributed on the entire sample.

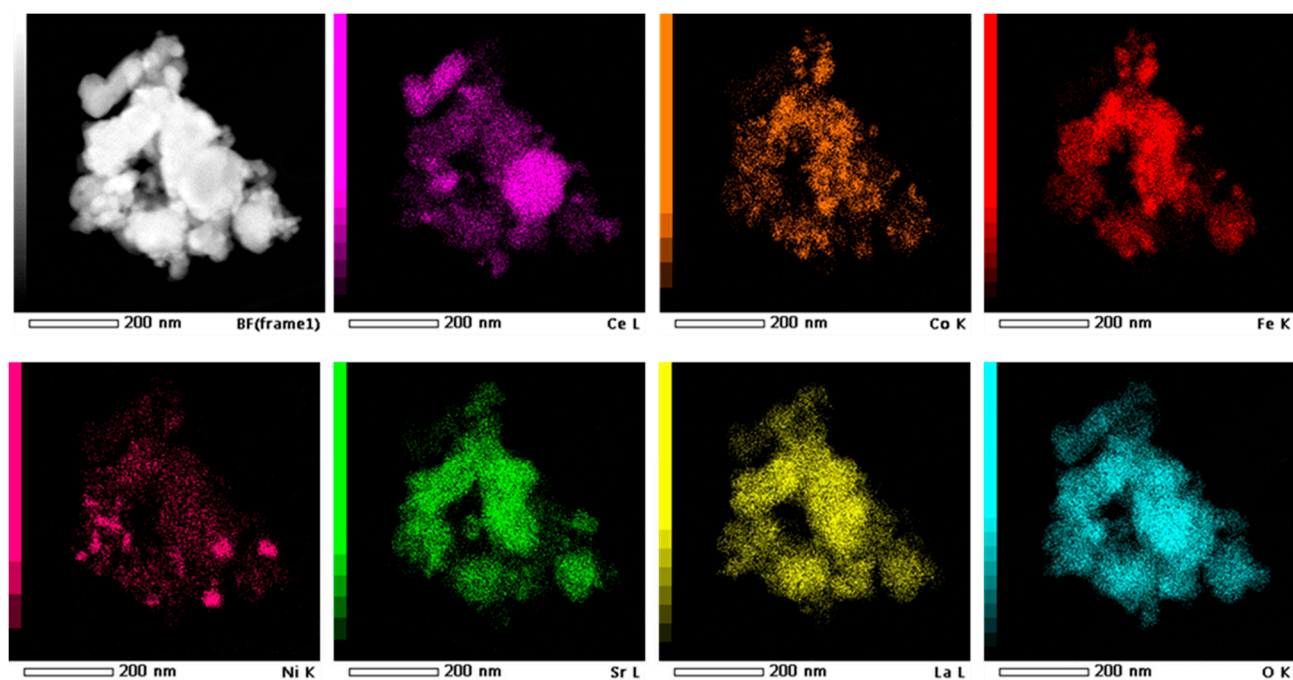


Figure S9. EDX analysis of spent functional layer.

## References

1. Faro, M.L.; Zignani, S.; Trocino, S.; Antonucci, V.; Aricò, A. New insights on the co-electrolysis of CO<sub>2</sub> and H<sub>2</sub>O through a solid oxide electrolyser operating at intermediate temperatures. *Electrochimica Acta* **2019**, *296*, 458–464, doi:10.1016/j.electacta.2018.11.079.
2. Faro, M.L.; Trocino, S.; Zignani, S.; Antonucci, V.; Aricò, A.S. Production of syngas by solid oxide electrolysis: A case study. *Int. J. Hydrogen Energy* **2017**, *42*, 27859–27865, doi:10.1016/j.ijhydene.2017.06.157.
3. Faro, M.L.; Da Silva, W.O.; Barrientos, W.V.; Saglietti, G.; Zignani, S.; Ticianelli, E.; Antonucci, V.; Aricò, A. The role of CuSn alloy in the co-electrolysis of CO<sub>2</sub> and H<sub>2</sub>O through an intermediate temperature solid oxide electrolyser. *J. Energy Storage* **2020**, *27*, 100820, doi:10.1016/j.est.2019.100820.
4. Vecino-Mantilla, S.; Quintero, E.; Fonseca, C.; Gauthier, G.H.; Gauthier-Maradei, P. Catalytic Steam Reforming of Natural Gas over a New Ni Exsolved Ruddlesden-Popper Manganite in SOFC Anode Conditions. *ChemCatChem* **2020**, *12*, 1453–1466, doi:10.1002/cctc.201902306.
5. Kim, J.S.; Lee, J.Y.; Swinnea, J.S.; Steinfink, H.; Reiff, W.M.; Lightfoot, P.; Pei, S.; Jorgensen, J.D. Ruddlesden-Popper phases A<sub>n+1</sub>M<sub>n</sub>O<sub>3n+1</sub>. Structures and properties, Paper presented at Proceedings of the International Conference on the Chemistry of Electronic Ceramic Materials, Jackson, WY, USA, 17–22 August 1990; pp. 301–306.
6. Lee, D.; Lee, H.N. Controlling Oxygen Mobility in Ruddlesden-Popper Oxides. *Mater.* **2017**, *10*, 368, doi:10.3390/ma10040368.
7. Smith, R.D.L.; Prévot, M.S.; Fagan, R.D.; Zhang, Z.; Sedach, P.A.; Siu, M.K.J.; Trudel, S.; Berlinguette, C.P. Photochemical route for accessing amorphous metal oxide materials for water oxidation catalysis. *Science*, **2013**, *340*, 60–63. doi: 10.1126/science.1233638.
8. Smith, R.D.L.; Prévot, M.S.; Fagan, R.D.; Trudel, S.; Berlinguette, C.P. Water oxidation catalysis: electrocatalytic response to metal stoichiometry in amorphous metal oxide films containing Iron, Cobalt, and Nickel, *Journal of the American Chemical Society*, **2013**, *135*, 11580–11586, doi.org/10.1021/ja403102j.